Bone xxx (xxxx) xxxx

Contents lists available at ScienceDirect

Bone

journal homepage: www.elsevier.com/locate/bone

Topology of microfractures in osteonecrotic femoral heads at μCT and histology

Charbel Mourad[a,b,*], Christine Galant[b,c], Emilie Wacheul[c], Thomas Kirchgesner[b,d], Nicolas Michoux[b,d], Bruno Vande Berg[b,d]

[a] Department of Radiology, Hôpital Libanais Geitaoui-CHU, Achrafieh, 1100 Beyrouth, Lebanon
[b] Institut de Recherche Expérimentale et Clinique (IREC), Université Catholique de Louvain, 55 Avenue Hippocrate, 1200 Woluwé-Saint-Lambert, Brussels, Belgium
[c] Department of Anatomopathology, Cliniques Universitaires Saint Luc, 10 Avenue Hippocrate, 1200 Woluwé-Saint-Lambert, Brussels, Belgium
[d] Department of Radiology, Cliniques Universitaires Saint Luc, 10 Avenue Hippocrate, 1200 Woluwé-Saint-Lambert, Brussels, Belgium

ARTICLE INFO

Keywords:
Osteonecrosis
Epiphyseal collapse
Microfracture
μCT
Histology

ABSTRACT

Aim: To assess the topology of bone and cartilage microfractures in osteonecrotic femoral heads.
Method: Sixteen resected human femoral heads with collapsed osteonecrosis (ON, $n = 11$) or osteoarthritis (OA, $n = 5$) were imaged at μCT with 12 μ nominal resolution. Forty-seven histological sections and μCT reformats with ($n = 30$) or without (8 from ON and 9 from OA femoral heads) osteonecrotic lesions were obtained and divided in 2 × 2 mm segments by a superposed grid. A radiologist and a pathologist separately assessed the presence of bone and cartilage microfractures in each segment on μCT and histological images, respectively. We determined the frequency and distribution of segments with bone microfractures according to a zonal distribution. Matrix analysis was performed by using Matlab to calculate the connectivity index and long/short axis ratios of clustered segments with microfractures.
Results: Segments with bone microfractures but not with cartilage microfractures were found more frequently in ON than in OA femoral heads. In the 38 matched μCT and histological images from ON femoral heads, 86%/82% of segments with cortical microfracture, 91%/96% of segments with trabecular microfractures involved ON lesions at μCT/histology. At histology, 83% of segments with cartilage microfractures involved ON lesions. In the 30 paired μCT and histological images containing necrotic lesions, the frequency of segments with trabecular microfractures in the superficial layers (55% at μCT/51% at histology) was statistically significantly higher than in the deep layer (25% $P < 0.0001$/35%; $P = 0.0006$). Clustered segments with cortical/trabecular microfractures, exclusively found in osteonecrotic lesions, had a connectivity index > 2.0/20.0 and mean long/short axis ratio > 2.35/2.2, respectively.
Conclusion: Segments with bone microfractures predominate in necrotic lesions. Segments with trabecular microfractures form elongated clusters near the femoral head surface.

1. Introduction

Epiphyseal collapse refers to the spontaneous failure of the subchondral bone plate and underlying bone appearing in an non-traumatic setting frequently, but non exclusively, in osteonecrosis [1]. Cartilage and bone fractures along with bone resorption have been described in epiphyseal collapse on radiographs [2–4]. In clinical practice, magnetic resonance imaging (MRI) is the modality of choice to diagnose femoral head osteonecrosis (ON). However, staging of femoral head osteonecrosis using MRI remains challenging as early femoral head collapse detected on CT imaging can be missed on MRI [2]. In addition, interobserver reproducibility of femoral head ON staging with MRI has been consistently found limited [5–8]. Therefore, there is a need for a better understanding of epiphyseal fracture and collapse.

Histological analysis of resected osteonecrotic (ON) femoral heads has demonstrated the presence of fibrovascular tissue at the periphery and within ON lesion associated with bone sclerosis or resorption [9–14] The topology of cortical and trabecular bone changes has received little attention. The usual histomorphometry technique that enables a better analysis of the mineralized bone requires prior fixation

Abbreviations: ON, osteonecrosis; OA, osteoarthritis; μCT, microcomputed tomography; FH, femoral head

* Corresponding author at: Department of Radiology, Hôpital Libanais Geitaoui-CHU, Achrafieh, 1100 Beyrouth, Lebanon.
E-mail addresses: charbel.mourad@uclouvain.be (C. Mourad), christine.galant@uclouvain.be (C. Galant), Emilie.wacheul@uclouvain.be (E. Wacheul), Thomas.kirchgesner@uclouvain.be (T. Kirchgesner), Nicolas.michoux@uclouvain.be (N. Michoux), Bruno.vandeberg@uclouvain.be (B. Vande Berg).

https://doi.org/10.1016/j.bone.2020.115623
Received 6 July 2020; Received in revised form 14 August 2020; Accepted 28 August 2020

in methylmetacrylate resin, rendering a subsequent decalcification and histological analysis impossible. Microcomputed tomography (μCT) is a high-resolution imaging technique that enables the analysis of the architecture of the mineralized bone with possible subsequent histological processing of the same specimen. μCT of resected osteonecrotic femoral heads demonstrated quantitative histomorphometric bone changes with little information on cortical and trabecular bone microfracture [15–19]. The aim of the current study was to assess the topology of bone and cartilage microfractures in resected human femoral heads with osteonecrosis (ON) at μCT and histology to contribute to a better understanding of the failure pattern of the femoral head osteonecrosis.

2. Material and methods

2.1. Patients population

The IRB of the institution approved the study, with the informed consent of the patients being waived. Between September 2015 and October 2017, a fellow in musculo-skeletal radiology collected 11 consecutive femoral head specimens with ON (6 men (mean age (range): 46.5 years; 30–67 years) and 5 women (68.6 years; 43–85 years)) resected for total hip replacement. Meanwhile, he also collected five femoral head specimens with OA (2 men and 3 women, (72.2 years; 40–90 years) (Fig. 1). Causes for ON included steroid (n = 5), alcohol abuse (n = 1) or was idiopathic (n = 5). Preoperative diagnosis of ON was based on radiographs (n = 9; mean delay between radiographs and surgery of 48 days (range: 1–132)) and on MRI (n = 6; mean delay between MRI and surgery of 75 days; range:2–194). All ON femoral heads demonstrated collapse at pre-operative imaging including five ARCO 3-early, five ARCO 3-late and one ARCO 4 osteonecrotic femoral heads [20]. After resection, all femoral head specimens were fixated in a formalin buffered solution.

2.2. μCT imaging and histological preparation

The same radiologist sawed the 16 femoral heads (EXAKT 312 diamond band saw, Germany) according to preoperative imaging to obtain 28 blocks of 2 × 2 cm (1.75 blocks per specimen; min 1; max 3). The 28 blocks were scanned by using a μCT scanner (SkyScan 1173 microtomograph, Bruker Company, Kontich, Belgium) at a nominal resolution of 12 μm (90 kV; Al filter; no pixel binning; scan orbit 360°; rotation step 0.2°; voxel volume: 1.728 10^{-9} ml; duration: 120 min) [21]. The blocks were decalcified with a formamide solution for 24 h and embedded in paraffin. Forty-seven histological sections were obtained by the same radiologist and processed for microscopic analysis (Fig. 1). The number of sections (1 to 3 sections per specimen) varied depending on the size of the osteonecrotic lesion. There were 30 slabs with ON lesions obtained from ON femoral heads and 17 slabs without ON lesions obtained from ON femoral heads (n = 8) or from OA femoral heads (n = 9). These 47 histological sections were selected according to μCT imaging of the whole femoral head to include the different regions of the osteonecrotic lesion (within the necrosis, at the interface and outside necrosis), the different bone components (cartilage, cortical and trabecular bone) and to avoid artifacts related to surgery. The 47 5-microns thick sections were cut, mounted on glass slides, stained with Hematoxylin and Eosin and digitized (Hamamatsu Nano Zoomer 2.0 rs.) at a resolution equivalent to an x40 optical magnification. The 47 histological images were viewed on dedicated software (Nanozoomer Digital Pathology Viewer 2.6.8, Hamamatsu Photonics K.K., 2016) and a 2-mm scale bar was inserted in the images. For each histological section, the same radiologist obtained a μCT reformat that matched the digitized histological section by using a landmark-based manual processing using a multiplanar reconstruction software (Dataviewer Bruker Dataviewer version 1.5.4.0, Bruker, Kontich, Belgium) as previously described [21]. A 2-mm scale bar was inserted in every image.

2.3. Image segmentation and labelling of segments

The 47 matched μCT and histology images were segmented by applying a transparent grid on each image (Microsoft PowerPoint) and were identically magnified so that the 2 × 2 mm scale on the images corresponded to one grid square (Figs. 2, 3 and 4). In the 38 matched μCT/histological images from the ON femoral head specimens, there were 2107 segments (mean +/-SD per specimen: 55.45 ± 12.57; range: 25–88) that contained cortical bone (n = 343), trabecular bone (n = 1740) and articular cartilage (n = 444). In the nine matched μCT/histological images from the OA femoral head specimens, there were 395 segments (43.9 ± 15.2 range: 26–76) that contained cortical (n = 67) or trabecular bone (n = 304) and articular cartilage (n = 72). Segments whose surface contained less than 25% of tissue were

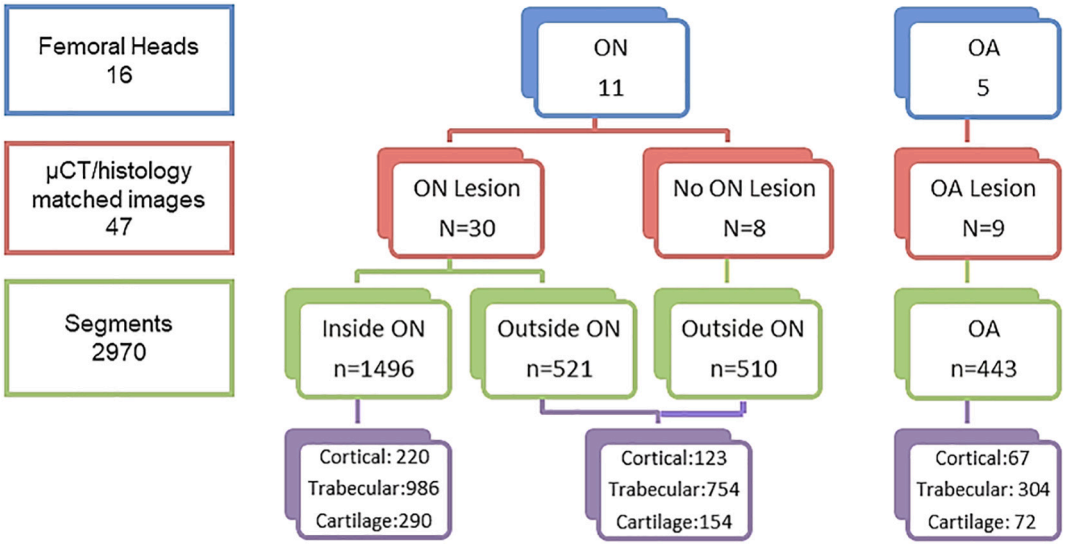

Fig. 1. Flowchart of the study material indicating the number of resected femoral heads with osteonecrosis (ON) and osteoarthritis (OA), the number of matched μCT and histology images, the number of segments with or without necrotic lesion and the number of segments containing cortical bone, trabecular bone and hyaline cartilage.

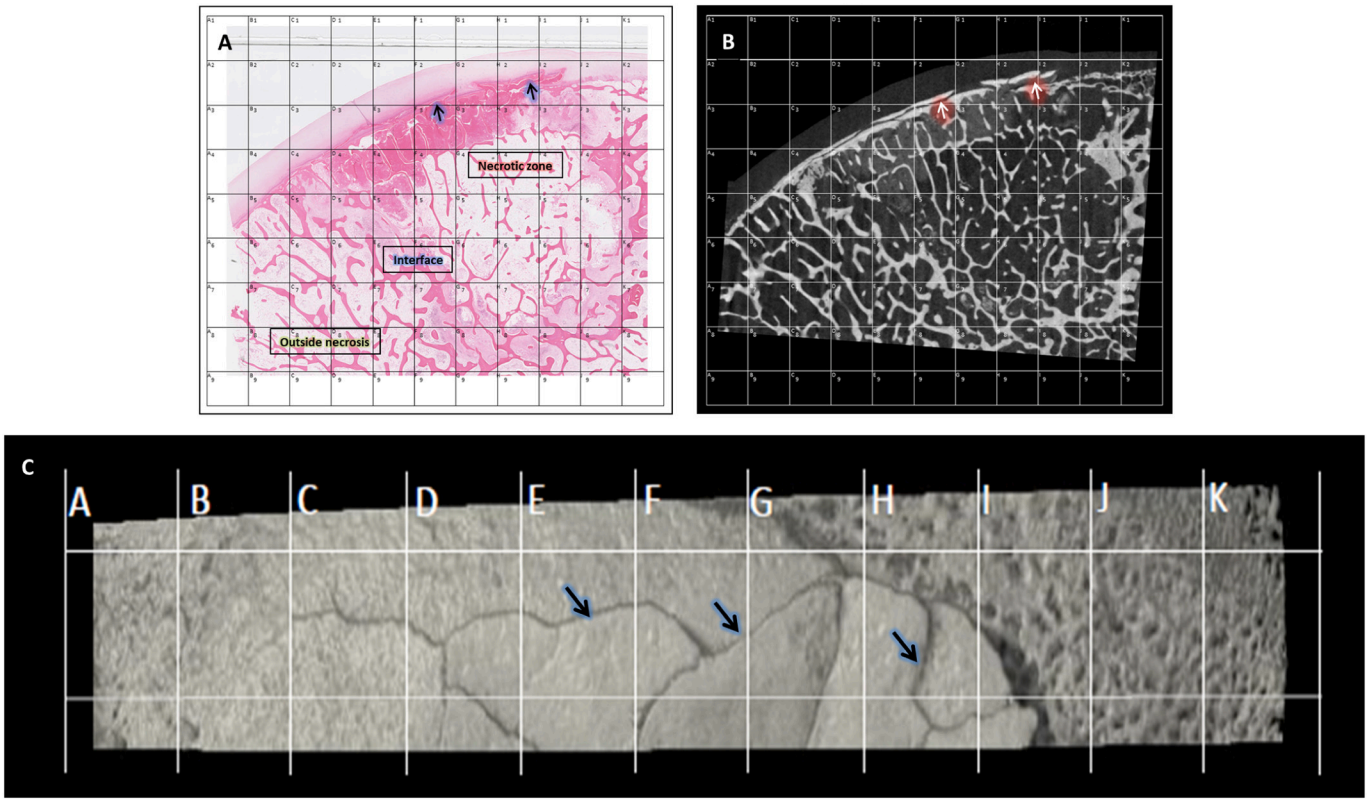

Fig. 2. 30-year-old man with left hip steroid-induced osteonecrosis (ARCO stage 3-late). (A) Low magnification histological section (H&E stain) of the resected femoral head specimen with superimposed grid, and corresponding μCT(B). Multiple microfractures of the cortical bone of the subchondral bone plate are well depicted (arrows in A and B). (C) surface 3D μCT view shows cortical microfractures (arrows).

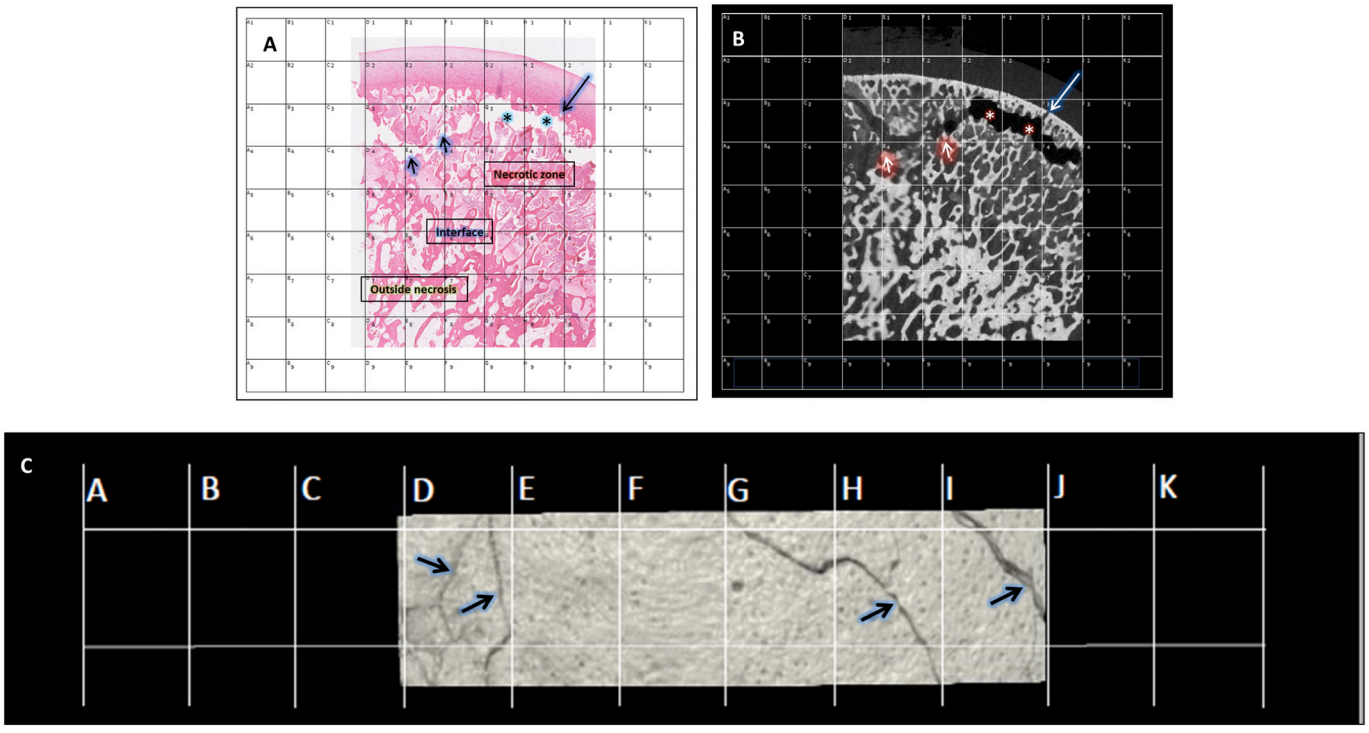

Fig. 3. 43-year- old woman with left hip osteonecrosis (ARCO stage 3-early). (A) Low magnification histological section (H&E stain) of the resected femoral head specimen with superimposed grid, and corresponding μCT (B) showing microfractures of the trabecular bone in the superficial (asterisks) and deep layers (arrows) of the necrotic zone. (C) surface 3D μCT view shows associated cortical microfractures (arrows).

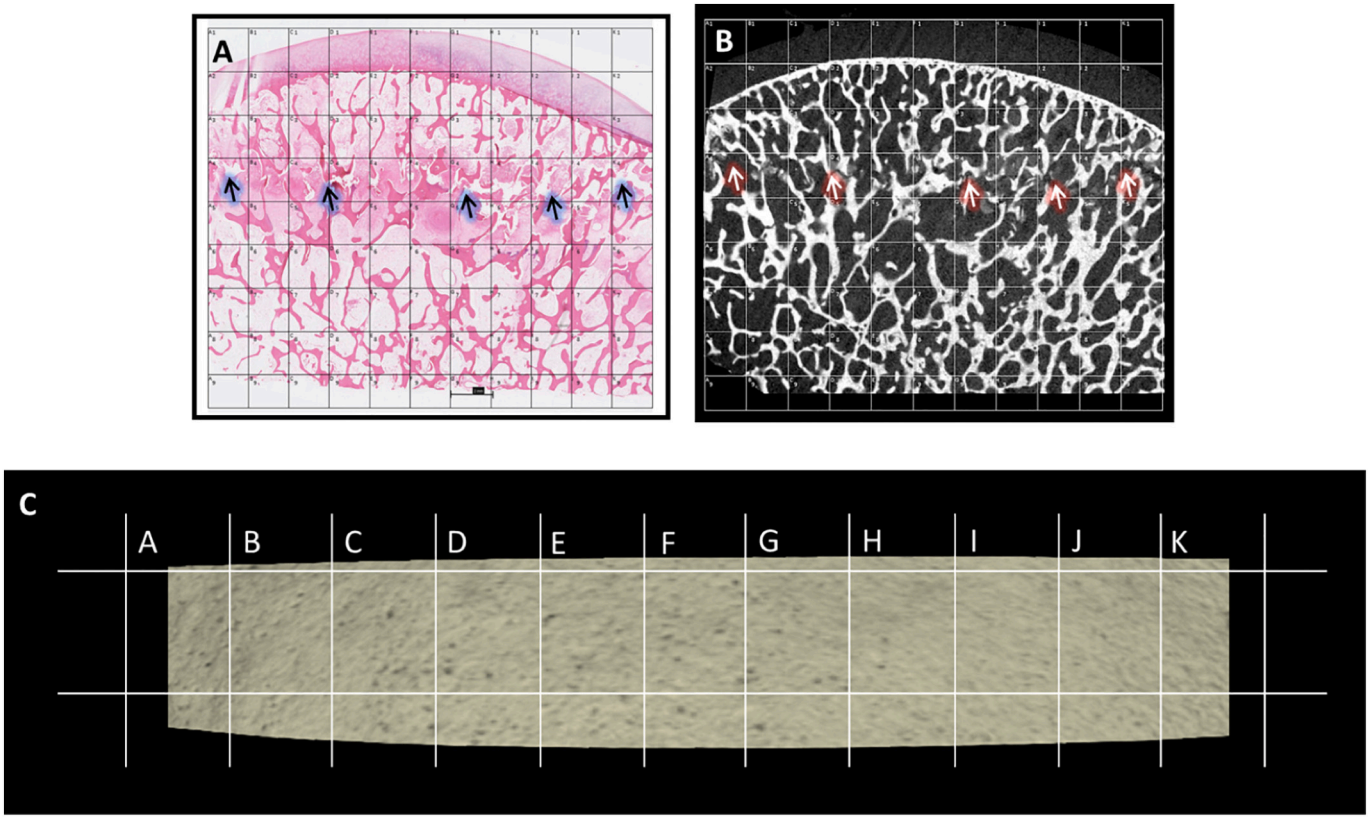

Fig. 4. 37-year-old man with right hip steroid-induced osteonecrosis (ARCO stage 3-early). (A) Low magnification histological section (H&E stain) of the resected femoral head specimen with superimposed grid, and corresponding μCT (B), showing trabecular microfracture along the reactive interface (arrows). (C) surface 3D μCT view shows the lack of cortical bone microfracture.

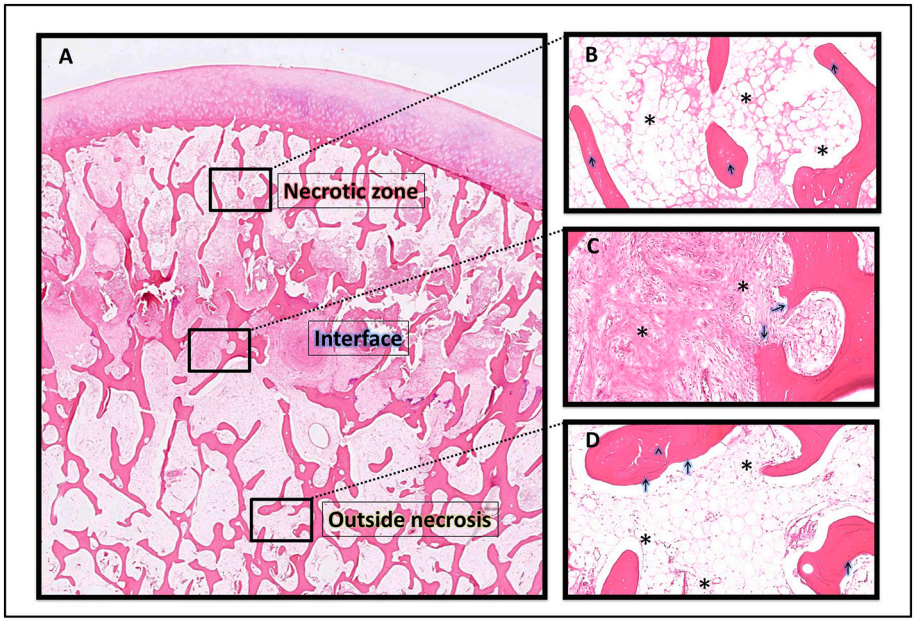

Fig. 5. 37-year-old man with right hip steroid induced osteonecrosis (ARCO stage 3-early). (A) A low magnification histological section (H&E stain) of the resected femoral head specimen shows the zonal distribution of the osteonecrotic lesion. (B) High magnification view of the necrotic zone shows empty osteocyte lacunae (arrows), dead adipocytes with absent nuclei (asterisks). (C) High magnification view of the reactive interface shows resorbed edges of the trabeculae (arrows) and reactive bone marrow (asterisks) rich in fibrovascular tissue. (D) High magnification view of the viable bone outside osteonecrotic lesion shows apposition of viable bone (arrows) on dead trabeculae with empty osteocyte lacunae (arrowhead), and viable bone marrow with normal adipocytes (asterisks).

excluded. The μCT and histological images were translated and rotated so that each segment of the grid contained the same areas of the μCT and histological images. Images were separately saved in a PDF format (Figs. 2, 3 and 4).

A pathology resident analyzed the 47 histological sections using a microscope and labelled each segment according to its dominant histological content and location with respect to the articular surface. Segments containing hyaline cartilage or cortical bone were all superficial and classified in three histological patterns based on the microscopic appearance of the adjacent bone and marrow including necrotic tissue, reactive interface or viable tissue as described below [9–14]. Segments containing trabecular bone were classified according to location and the same histological patterns. Superficial segments were located within two millimeters below the cortical bone covered by hyaline cartilage and deep segments were located deeper. Three histological patterns were defined as follows [11,22]. Necrotic tissue

consisted of necrotic trabeculae with saponified or mummified bone marrow necrosis [10,12,23]. Scattered empty osteocytes lacunae within trabeculae embedded in viable marrow were not considered to represent necrotic tissue [9,10,12,24]. The reactive interface consisted of a layer of fibrovascular connective tissue with trabecular bone resorption or sclerosis surrounding necrotic tissue [12]. Viable tissue consisted of normal bone and marrow devoid of necrotic or fibrovascular tissue that was located at distance from the ON lesion (Fig. 5). Some segments were assigned to different categories depending on the presence of cartilage, cortical and trabecular bone.

2.4. Lesion definition and image analysis

In December 2018 and January 2019, a musculoskeletal radiologist with 28 years of experience who was blinded to the histological findings analyzed the 47 µCT images to assess cartilage, cortical bone and trabecular bone microfractures. During the same period, a bone pathologist with 25 years of experience who was blinded to the µCT images analyzed the 47 histological images to assess cartilage, cortical and trabecular bone microfractures. Readers were blinded to clinical information and pre-operative findings. For each matched image, the same list of segments to be analyzed (identified by letters and numbers) was given to the readers. For each segment, readers documented the likelihood for the presence of cartilage or bone fracture by using a four-point Likert scale (0 = not present, 1: probably not present, 2: probably present, 3: present).

Lesions were defined as follow: Fracture of the cortical bone of the subchondral bone plate was defined as a focal linear full-thickness interruption of the cortical bone with or without angulation/displacement of the edges of the fracture at histology and at µCT (Figs. 2,3, 4 and 6). The presence of smooth focal deformation of the subchondral bone plate without interruption was not considered to be a fracture. At histology, the presence of adjacent tissue alterations was used to differentiate non-displaced fractures from physiological interruptions of the subchondral bone plate that contained marrow and normal vessels. Fracture of the trabecular bone was defined by the presence of sharp or irregular interruption of at least two adjacent trabeculae with or without displacement (Figs. 2,3, 4 and 6). The presence of small bone fragments clustered in a limited area was also considered to represent fractures even in the absence of interrupted trabeculae. Smooth interruption of the trabeculae was considered a normal finding. Longitudinal vertical cracks along cement lines within the trabeculae were not considered. When a microfracture occurred at the intersection of two adjacent segments, the closest segment to the articular surface was considered positive for fracture to avoid an artificial increase in microfracture number. Fracture of the articular cartilage was defined as a full-thickness linear interruption of the cartilage tissue at histology [4] and at µCT (Fig. 6). Cartilage changes due to degeneration were not taken into consideration. Folds, lines, tissue retraction, chatter, or crushing at the trajectory of surgical instruments were considered to represent artifacts. The two readers trained during a common session to reach agreement upon lesion criteria by analyzing five pairs of µCT/histological images that were not included in the study material.

Two months after their readings were completed, the two readers separately analyzed 20 randomly selected matched µCT and histological images from the study series to determine intra-observer agreement. At the end of the reading process, data was tabulated in Excel sheet and binarized as follows: an answer of 0 or 1 on the Likert scale was considered as negative for fracture; an answer of 2 or 3 was considered as positive for fracture.

2.5. Grid cell topology of segments with microfractures

For each 47 µCT and 47 histological images, a statistician created two matrices including all segments with cortical or trabecular bone. Segments containing cartilage fractures at histology were not analyzed because of their limited numbers. Results of readings were encoded in the corresponding matrices. Pixels with “1” corresponded to segments with microfracture and pixels with “0” corresponded to segments without microfracture. The 94 µCT matrices including the 47 matrices for cortical bone microfractures and 47 matrices for trabecular bone microfractures matrices and the corresponding 94 histological matrices were analyzed using the function *regionprops* of Matlab (Matlab version R2017a, MathWorks) to calculate several parameters (Table 1). An 8-connected pixel two-dimensional connectivity model was used, defined as follows: pixels are connected if their edges or corners touch. Two adjoining pixels are part of the same object if they are both on and are connected along the horizontal, vertical, or diagonal direction (Fig. 7). The parameter tends to 1 when the shape of the cluster tends to a circle and becomes superior to 1 if the cluster is elongated.

2.6. Statistical analysis

The frequency of segments with cortical, trabecular and cartilage microfracture at µCT and at histology was determined in the different zones of ON lesions and in OA lesions. The frequency of trabecular microfracture in the superficial layer of the ON lesions was compared with that in the deep layers of the lesions by using Chi-squared test. The percentage of agreement on a square by square basis was calculated between µCT and histological readings for the detection of cortical, trabecular and cartilage fracture in all the specimens. Kappa values were calculated and levels of agreement were interpreted using the mean value of the confidence interval according to the scale proposed by Altman (< 0,20: *poor*; 0,21-0,40: *fair*; 0,41-0,60: *moderate*; 0,61-0,80: *good*; 0,81-1,00: *very good*) [25]. The connectivity parameters of segments with cortical and trabecular microfracture in ON lesions were

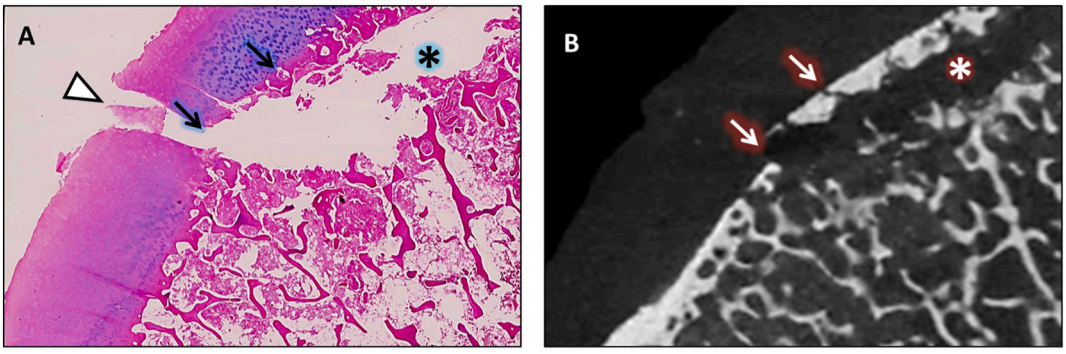

Fig. 6. 73-year-old woman with idiopathic osteonecrosis. Low magnification histological section (H&E stain) (A) and corresponding reformatted µCT image (B) of resected femoral head specimen with osteonecrosis. The fracture of the cartilage is visualized only on histology (arrowhead in A). Multiple cortical (arrows) and trabecular subchondral (asterisk) micro-fractures are well visible on both images.

Table 1
Definitions of the connectivity parameters calculated for the clustered segments with microfractures.

Parameter	Abbreviation	Definition
Largest cluster of microfractures	LC	Corresponds to the largest number of connected pixels with microfractures in every matrix. Pixels are connected if their edges or corners touch. Two adjoining pixels are part of the same cluster if they are both on and are connected along the horizontal, vertical, or diagonal direction
Number of clusters	$N^{cluster}$	The number of cluster of segments with microfractures regardless of their size.
Surface of the largest cluster	$Surface^{LC}$	Measures the actual number of segments with microfracture in the largest cluster of microfractures present in the matrix.
Sum of the connectivity in the largest cluster	$SumConnectivity^{LC}$	Measures, for each pixel with microfracture, the number of neighboring lesional pixels using an 8-connectivity model, then summing all numbers. As the parameter increases, the more *Blob*-like is the shape of the cluster, and/or the larger the cluster is.
Major axis of the largest cluster	$Major\ axis^{LC}$	Measures the length, in pixels, of the major axis of an ellipse with the same normalized second central moments as the largest cluster of microfractures.
Minor axis of the largest cluster	$Minor\ axis^{LC}$	Measures the length, in pixels, of the minor axis of an ellipse with the same normalized second central moments as the largest cluster of microfractures.
Ratio major axis/minor axis	$Ratio^{LC}$	Measures the ratio Major axis/Minor axis. The parameter tends to 1 when the shape of the cluster tends to a circle, and becomes superior to 1 if the cluster is elongated.

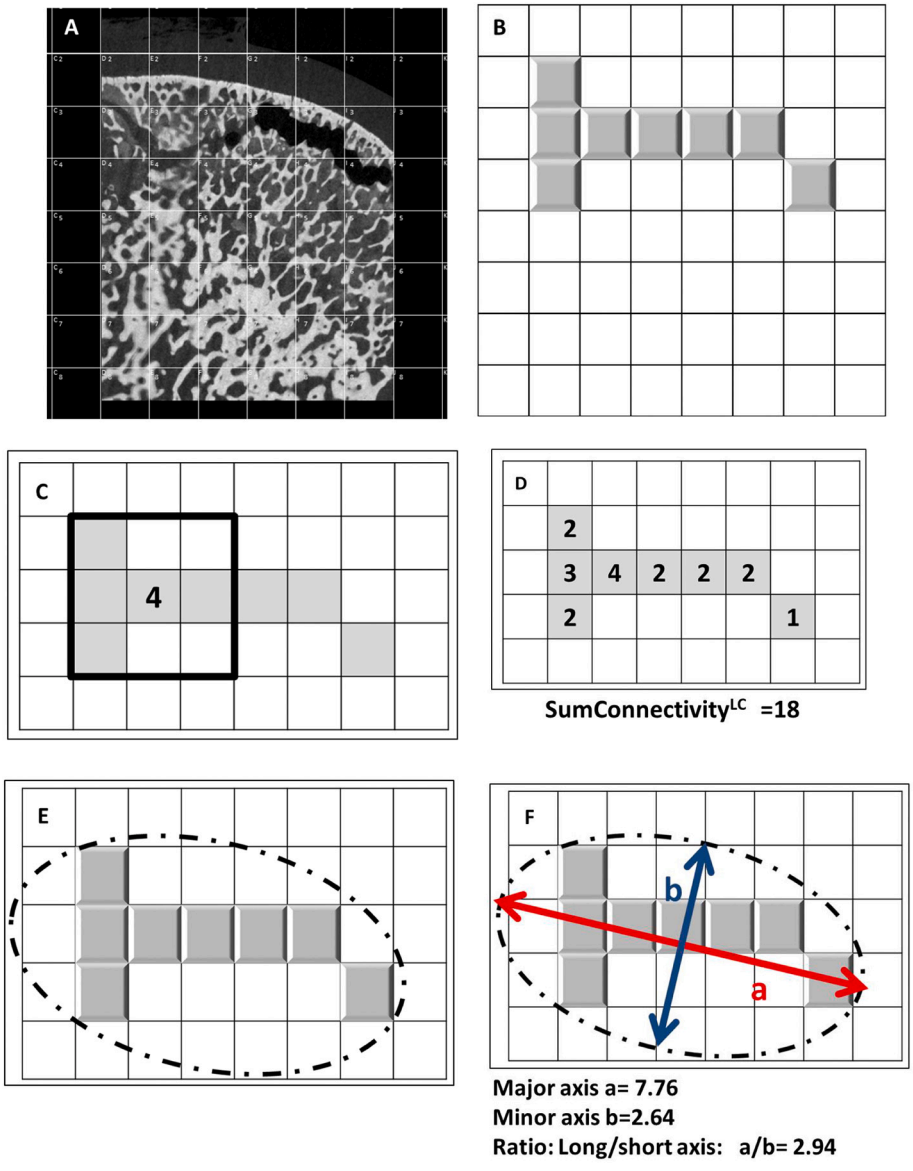

Fig. 7. 43-year old woman with left hip osteonecrosis (ARCO stage 3-early) (same as Fig. 3). (A) Reformatted 2D µCT image with a superimposed grid and (B) corresponding reading grid. Shaded gray segments contain trabecular microfractures. (C) and (D): Example of calculation of the 8-connected pixel two-dimensional connectivity model for a cluster of microfractures. The pixel (arrow in C) is in contact with 4 adjacent lesional pixels by its edges or corners. (D) the "$SumConnectivity^{LC}$" index corresponds to the sum of the connectivity of all the lesional pixels. (E) And (F): calculation of the Long/Short axis ratio of the cluster. (E) The best fitting ellipse is drawn around the cluster. (F) The parameter "$Ratio^{LC}$" corresponds to the ratio of the long (a) and short (b) axis of the ellipse.

Table 2
Frequency of segments with micro-fractures in 47 µCT reformats and corresponding histological slabs form osteonecrotic and osteoarthritic femoral heads. Segments with bone microfractures are more frequent in osteonecrotic than in osteoarthritic femoral heads.

	Frequency of segments with micro-fractures in			
	ON femoral heads (n = 11)		OA femoral heads (n = 5)	
	Number of µCT reformats (*n* = 38)	Number of histology sections (*n* = 38)	Number of µCT reformats (n = 9)	Number of histology sections (*n* = 9)
Cortical bone	29% [99/343]	32% [109/343]	7.5% [5/67]	3% [2/67]
Trabecular bone	15% [265/1740]	17% [305/1740]	3% [9/304]	1% [3/304]
Cartilage	0% [0/444]	5% [23/444]	0% [0/72]	4% [3/72]

ON Osteonecrotic; OA osteoarthritic; Percentages represent the frequency of segments with microfracture among all segments with cortical bone, trabecular bone or cartilage.

compared with those observed in specimens outside ON lesions and with OA by using Chi-squared test.

3. Results

3.1. Frequency of segments with microfractures in ON and OA femoral heads

In the 38 matched µCT and histological images obtained from ON femoral heads, 29% and 32% of the 343 segments containing cortical bone demonstrated cortical bone microfractures at µCT and histology, respectively (Table 2). 15% (µCT) and 17% (histology) of the 1740 segments containing trabecular bone demonstrated trabecular bone microfractures. 0% (µCT) and 4% (histology) of the 444 segments containing cartilage demonstrated cartilage microfractures. In the 9 matched µCT and histological images obtained from OA femoral heads, a limited number of segments contained microfractures (Tables 2, 3). Segments with cortical and trabecular microfractures were statistically significantly more frequent in ON than in OA specimens at µCT and histology ($p < 10^{-3}$ for both techniques). There was no statistically significant difference in frequency of cartilage microfracture between ON and OA specimens at histology.

3.2. Distribution of segments with microfractures in ON femoral heads

In the 38 matched µCT and histology images obtained from ON specimens, 86% and 82% of segments with cortical bone microfracture and 91% and 96% of segments with trabecular microfractures were located in ON lesions at µCT and histology, respectively (Table 4). At histology, 83% of segments with cartilage microfractures were found in osteonecrotic lesions.

In the 30 matched µCT and histology images containing necrotic lesions, the frequency of segments with cortical microfractures was statistically significantly higher in the necrotic region than in the interface ($p < 10^{-3}$ for µCT and histology) (Table 5). The frequency of segments with trabecular microfractures was statistically significantly higher in the superficial than in the deep layer in the necrotic tissue ($p < 10^{-3}$ for both techniques) and in the interface ($p < 10^{-4}$ at µCT and $p = 0.02$ at histology) (Table 5).

3.3. Clustering of segments with bone microfractures

Clusters of segments with bone microfractures were found exclusively in osteonecrotic lesions, with a mean number of segments with cortical microfracture of 2.0 (µCT) and 2.83 (histology) and a mean number of segments with trabecular microfracture of 7.4 and 8.5. (Table 6). The mean of the sum of the connectivity of the clustered segments with trabecular microfracture was 23 at µCT and 29 at histology (Table 6). The mean of the long/short axis ratio of the clustered segments with trabecular microfracture was 2.4 at µCT and 2.2 at histology (Table 6).

3.4. Correlations between µCT and histology

The percentage of agreement between µCT and histology was 82% for cortical bone microfracture (kappa = 0.54 [0.44–0.63] and 87% for trabecular bone microfracture (kappa = 0.48[0.43–0.54]. At µCT, intraobserver agreement was good for the detection of cortical (kappa = 0.725) and trabecular (kappa = 0.751) microfractures. At histology, intraobserver agreement was good for the detection of segments with cortical bone microfractures (kappa = 0.66) and moderate for that of segments with trabecular bone microfracture (kappa = 0.498).

4. Discussion

The current study paved the way for a quantitative assessment of microfracture topology in femoral heads at µCT and histology and yields three main results. First, segments with bone-but not with cartilage-microfractures were found more frequently in ON than in OA femoral heads and, in the former case, largely predominated in the necrotic lesions. Second, in ON femoral heads, segments with trabecular microfractures were found in all zones of the necrotic lesions but their frequency was higher in the superficial subchondral layer than in the deep layer. Finally, segments with bone microfractures formed elongated clusters only in necrotic lesions and predominated near the femoral head surface.

Several theories may explain epiphyseal collapse in ON. According

Table 3
Frequency of segments with microfractures in superficial and deep zones of 9 µCT reformats and corresponding histological images from OA femoral heads.

	Cortical bone segments (n = 67)		Trabecular bone segments (n = 304)		Cartilage segments (n = 72)	
	Segments with µ# at µCT (n = 5)	Segments with µ# at histology (*n* = 2)	Segments with µ# at µCT (n = 9)	Segments with µ# at histology (n = 3)	Segments with µ# at µCT (*n* = 0)	Segments with µ# at histology (n = 3)
Superficial zone	7.5% (5/67)	3% (2/67)	4% (3/71)	0% (0/71)	0% (0/72)	4% (3/72)
Deep zone	NA	NA	2.5% (6/233)	1.3% (3/233)	NA	NA

NA Not applicable; µ# microfracture; Percentages correspond to the proportion of segments with microfractures among all segments containing cortical bone, trabecular bone or cartilage within each zone.

Table 4
Distribution of segments with bone microfractures in necrotic and in non-necrotic zones in 38 µCT reformats and 38 corresponding histological sections from osteonecrotic femoral heads. Segments with microfractures predominate in ON lesions. Trabecular microfractures involve the superficial and the deep layers of the lesions.

		Cortical bone segments (n = 343)		Trabecular bone segments (n = 1740)	
		Segments with µ# at µCT (*n* = 99)	Segments with µ# at histology (*n* = 109)	Segments with µ# at µCT (*n* = 265)	Segments with µ# at histology (*n* = 305)
In ON lesion	Superficial zone	86% (85/99)	82% (90/109)	37% (99/265)	29% (89/305)
	Deep zone	NA	NA	54% (143/265)	67% (205/305)
Out of ON lesion	Superficial zone	14% (14/99)	17% (19/109)	5% (14/265)	3% (9/305)
	Deep zone	NA	NA	3% (9/265)	1% (2/305)

NA not applicable; ON osteonecrotic; µ# microfracture. Percentages correspond to the proportion of segments with microfractures among all segments with microfracture.

Table 5
Frequency (in %) of segments with microfractures in superficial and deep layers of the central necrotic tissue and marginal interface in 30 µCT reformats and 30 histological sections containing necrotic tissue from ON femoral heads. Microfractures are ubiquitous and predominate in superficial layers.

		Cortical bone segments (*n* = 220)		Trabecular bone segments (*n* = 986)		Cartilage segments (*n* = 290)	
		Segments with µ# at µCT (*n* = 85)	Segments with µ# at Histology (*n* = 90)	Segments with µ# at µCT (*n* = 242)	Segments with µ# at histology (*n* = 294)	Segments with µ# at µCT (n = 0)	Segments with µ# at histology (*n* = 19)
Necrotic tissue	Superficial zone	43% (68/158)	46% (73/158)	55% (82/148)	51% (75/148)	0% (0/231)	5% (16/231)
	Deep zone	NA	NA	25% (112/442)	35% (156/442)	NA	NA
Interface	Superficial zone	27% (17/62)	27% (17/62)	32% (17/53)	26% (14/53)	0% (0/59)	5% (3/59)
	Deep zone	NA	NA	9% (31/343)	14% (49/343)	NA	NA

NA not applicable; ON osteonecrotic; µ# microfracture; Percentages correspond to the proportion of segments with microfractures among all segments containing cortical bone, trabecular bone or cartilage within each zone.

to the "abnormal healing" theory, microfractures within necrotic bone do not heal and probably tend to accumulate and lead ultimately to overt fracture and subsequent collapse [26,27]. Our results support this theory by demonstrating that microfractures do occur in viable zones of ON femoral heads as in OA femoral heads, but at a much lower frequency than in necrotic lesions where they accumulate. In necrotic and in non-necrotic tissue, trabecular microfractures predominated in the superficial, subchondral layer of the trabecular bone were stresses are likely to predominate. According to the "abnormal stress" theory, trabecular microfracture could also occur in the peripheral areas of osteonecrotic lesions where bone changes -sclerosis or resorption - are likely to alter stress distribution, favoring microfracture development and propagation [15,28]. In agreement with that theory, 9% (µCT) and 14% (histology) of segments located at the interface also showed trabecular microfractures. An underestimation of these fractures is possible because bone resorption may cause fracture to become invisible or because fractures could heal in viable tissue.

The current study showed that segments with microfractures form elongated clusters in the necrotic areas but not in the viable areas outside necrosis or in OA specimens. This clustering phenomenon potentially reflects the predilection for microfracture to propagate, and that depends on numerous parameters including bulk material properties, microfracture geometry and stress distribution, magnitude and rate [29]. Despite the higher frequency of segments with microfractures in cortical than in trabecular bone, the mean number of segments per cluster was much lower for cortical bone than for trabecular bone microfractures reflecting fracture propagation in a plane (cortical bone) rather than in a volume (trabecular bone).

Finally, we demonstrated that frequency of segments with cartilage microfractures was very low both in ON and in OA femoral heads. In addition, no clustering of segments with cartilage microfractures was observed. These observations are in line with the fact that articular cartilage is relatively preserved until late in the ON disease course because of its resilient properties and its nutritional supply by the synovial fluid [14,30]. In the current study, we focused on cartilage microfractures and we did not assess degenerative changes and abrasion of the articular cartilage in ON and OA specimens. In some instances, limited areas of osteonecrosis may occur in femoral heads with osteoarthritis and this was not the case in our OA specimens [13,31].

In the current study, spatially matched µCT and histological images were used to detect microfractures and describe their topology. The µCT is a non-destructive technique that depicts the mineralized bone component with high spatial resolution without interference with a subsequent histological processing. The high spatial resolution of µCT is close to histology enabling a comparative evaluation of both techniques. The diagnostic performance of each technique for the detection of microfractures was not determined in the absence of a validated standard of reference to which both methods could be compared. Inter-technique agreement for the presence of microfractures was 82% for cortical and 87% for trabecular bone, indicating an acceptable diagnostic performance.

The current study has several limitations. First, because of the

Table 6
Connectivity parameters of the largest cluster^{LC} of segments with cortical and trabecular microfractures in osteonecrotic and osteoarthritic femoral heads at µCT and histology. Segments with microfractures form clusters and concentrate in the necrotic lesion. Outside the lesion, segments with microfractures are isolated and do not form clusters randomly distributed.

		Osteonecrotic femoral heads				Osteoarthritic femoral heads	
		Within ON lesion		Outside ON lesion			
		µCT	Histology	µCT	Histology	µCT	Histology
Cortical bone	$N^{cluster}$	1.24 [0.96;1.52]	1.24 [0.94;1.54]	0.75 [0.16;1.34]	1.25 [0.28;2.22]	0.63 [0.01;1.25]	0.00 [0.00;0.38]*
	$Surface^{LC}$	2.00 [1.00;3.00]*	2.83 [2.01;3.64]	1.00 [0.11;1.89]	0.88 [0.18;1.57]	0.50 [0.00;1.00]*	0.00 [0.00;0.19]
	$SumConnectivity^{LC}$	2.00 [0.00;4.00]*	2.00 [2.00;6.00]*	0.00 [0.00;2.38]*	0.00 [0.00;2.00]*	0.00 [0.00;0.00]*	0.00 [0.00;0.00]*
	$Major\ axis^{LC}$	2.31 [1.15;3.85]*	3.29 [2.35;4.23]	1.25 [0.11;2.38]	1.10 [0.16;2.05]	0.58 [0.00;1.15]*	0.00 [0.00;0.22]*
	$Minor\ axis^{LC}$	1.15 [1.15;1.15]*	1.20 [0.96;1.45]	0.72 [0.22;1.22]	0.72 [0.22;1.22]	0.58 [0.00;1.15]*	0.00 [0.00;0.22]*
	$Ratio^{LC}$	2.28 [1.65;2.92]	2.35 [1.75;2.96]	1.08 [0.10;2.06]	0.96 [0.14;1.77]	0.50 [0.00;1.00]*	0.00 [0.00;0.19]*
Trabecular bone	$N^{cluster}$	1.0 [1.0;2.0]*	1.8 [1.5;2.1]	0.0 [0.0;1.4]*	1.1 [0.4;1.8]	1.0 [0.0;1.0]*	0.0 [0.0;0.9]*
	$Surface^{LC}$	7.4 [5.6;9.2]	8.5 [6.9;10]	0.0 [0.0;2.6]*	0.9 [0.3;1.4]	1.0 [0.0;1.0]*	0.0 [0.0;0.9]*
	$SumConnectivity^{LC}$	23 [16;30]	29 [22;36]	0.0 [0.0;3.5]*	0.0 [0.0;0.4]*	0.0 [0.0;0.0]*	0.0 [0.0;0.0]*
	$Major\ axis^{LC}$	5.3 [4.3;6.4]	5.5 [4.8;6.3]	0.0 [0.0;2.9]*	1.2 [0.0;1.5]*	1.2 [0.0;1.2]*	0.0 [0.0;1.0]*
	$Minor\ axis^{LC}$	2.2 [1.8;2.6]	2.6 [2.3;2.9]	0.0 [0.0;1.3]*	1.2 [0.0;1.2]*	1.2 [0.0;1.2]*	0.0 [0.0;0.0]*
	$Ratio^{LC}$	2.4 [1.9;2.8]	2.2 [1.9;2.4]	0.0 [0.0;2.2]*	1.0 [0.3;1.6]	1.0 [0.0;1.0]*	0.0 [0.0;0.9]*

Mean value, *median value, with 95%CI in brackets.

limited number of specimens, our results lack statistical power to compare the frequency of microfractures between the different ARCO stages, or to correlate them with the ON etiology. In addition, no early stage femoral head osteonecrosis was included in our study as total hip replacement is usually performed in collapsed lesions. Second, we defined bone microfracture as full-thickness transverse interruption of the cortical and trabecular bone. Microcracks occurring within bone lamellae were not considered in the current study. Third, the lack of visibility of cartilage microfracture at µCT could have been related to the inability to modify the window width and levels on PDF images format. Prior staining of the cartilage surface with a radio-opaque dye could have increased the detection rate of cartilage microfracture at µCT [32,33]. Fourth, harvesting of the block specimens was performed according to the femoral head lesions by a radiology fellow who was aware of the imaging findings subsequent to the specimen sampling procedure. The distribution of microfractures was determined with respect to the osteonecrotic lesions and not to the anatomic segments of the involved femoral heads. Fifth, interobserver reproducibility for analysis of the µCT and histological images was not obtained because the radiology and pathology residents involved in the image preparation would not have been blinded readers given the limited number of specimens. Intraobserver reproducibility was determined and was good at µCT and moderate to good at histology.

In conclusion, cortical and trabecular bone microfractures are frequent in collapsed necrotic lesions and are ubiquitous. Trabecular microfractures predominate in the superficial layer of the epiphysis and form elongated clusters. Microfractures in viable areas of ON femoral heads and in OA femoral heads are scattered in the superficial subchondral areas of the femoral heads and do not form clusters.

CRediT authorship contribution statement

Mourad Charbel: Conceptualization; Methodology; Investigation: Software; Writing - original draft; review & editing. **Galant Christine**: Methodology; Investigation; Writing - review & editing. **Wacheul Emilie**: Investigation. **Kirchgesner Thomas**: Writing - review & editing. **Michoux Nicolas**: Formal analysis; Writing - review & editing. **Vande Berg Bruno**: Conceptualization; Methodology Writing - original draft; review & editing; Supervision.

Funding

This research did not receive any specific grant from funding agencies in the public, commercial, or not-for-profit sectors.

Declaration of competing interest

All the authors have nothing to disclose.

References

[1] T. Gorbachova, I. Amber, N.M. Beckmann, D.L. Bennett, E.Y. Chang, L. Davis, et al., Nomenclature of subchondral nonneoplastic bone lesions, Am. J. Roentgenol. 213 (5) (2019) 963–982.
[2] K.T Stevens .C.T., S.-U. Lee, N. Salem, J. Vandevenne, C. Cheng, G. Neumann, A_.-V. Opran, P. Lang, Subchondral fractures in osteonecrosis of the femoral head: comparison of radiography, CT, and MR imaging, AJR American journal of roentgenology 180 (2003) 363–368.
[3] M. Abumis H, M. Uetani, T. Yamaguchi, Bone marrow edema and subchondral fracture in osteonecrosis of the femoral head: analysis with MRI and CT, Acta Medica Nagasakiensia. 58 (1) (2013) 13–18.
[4] J.W. Milgram, Injury to articular cartilage joint surfaces: II. Displaced fractures of underlying bone. A histopathologic study of human tissue specimens, Clin. Orthop. Relat. Res. 206 (206) (1986) 236–247.
[5] R.M. Kay, J.R. Lieberman, F.J. Dorey, L.L. Seeger, Inter- and intraobserver variation in staging patients with proven avascular necrosis of the hip, Clin. Orthop. Relat. Res. 307 (1994) 124–129.
[6] S.W. Smith, R.A. Meyer, P.M. Connor, S.E. Smith, E.N. Hanley Jr., Interobserver reliability and intraobserver reproducibility of the modified Ficat classification system of osteonecrosis of the femoral head, J. Bone Joint Surg. Am. 78 (11) (1996) 1702–1706.
[7] A.Y. Plakseychuk, M. Shah, S.E. Varitimidis, H.E. Rubash, D. Sotereanos, Classification of osteonecrosis of the femoral head. Reliability, reproducibility, and

prognostic value, Clinical orthopaedics and related research 386 (2001) 34–41.
[8] M. Schmitt-Sody, C. Kirchhoff, W. Mayer, M. Goebel, V. Jansson, Avascular necrosis of the femoral head: inter- and intraobserver variations of Ficat and ARCO classifications, Int. Orthop. 32 (3) (2007) 283–287.
[9] M.J.K.J. Glimcher, Nicolas Andry award. The biology of osteonecrosis of the human femoral head and its clinical implications. 1. Tissue biology, Clin Orthop. 138 (1979) 284–309.
[10] C. Fondi, A. Franchi, Definition of bone necrosis by the pathologist, Clin Cases Miner Bone Metab. 4 (1) (2007) 21–26.
[11] M.D. Murphey, K.L. Foreman, M.K. Klassen-Fischer, M.G. Fox, E.M. Chung, M.J. Kransdorf, From the radiologic pathology archives imaging of osteonecrosis: radiologic-pathologic correlation, RadioGraphics. 34 (4) (2014) 1003–1028.
[12] M. Catto, Ischaemia of bone, J Clin Pathol Suppl (R Coll Pathol). 11 (1977) 78–93.
[13] C.F. Ilardi, L. Sokoloff, Secondary osteonecrosis in osteoarthritis of the femoral head, Hum. Pathol. 15 (1) (1984) 79–83.
[14] R.J. Patterson, W.H. Bickel, D.C. Dahlin, Idiopathic avascular necrosis of the head of the femur. A study of fifty-two cases, J. Bone Joint Surg. Am. 46 (1964) 267–282.
[15] H. Hamada, M. Takao, T. Sakai, N. Sugano, Subchondral fracture begins from the bone resorption area in osteonecrosis of the femoral head: a micro-computerised tomography study, Int. Orthop. 42 (7) (2018) 1479–1484.
[16] C. Wang, X. Wang, X.L. Xu, X.L. Yuan, W.L. Gou, A.Y. Wang, et al., Bone microstructure and regional distribution of osteoblast and osteoclast activity in the osteonecrotic femoral head, PLoS One 9 (5) (2014) e96361.
[17] C. Wang, Y. Wang, H. Meng, W. Gou, X. Yuan, X. Xu, et al., Microstructure and nanomechanical properties of single trabecular bone in different regions of osteonecrosis of the femoral head, J. Nanosci. Nanotechnol. 16 (3) (2016) 2264–2269.
[18] C. Wang, H. Meng, Y. Wang, B. Zhao, C. Zhao, W. Sun, et al., Analysis of early stage osteonecrosis of the human femoral head and the mechanism of femoral head collapse, Int. J. Biol. Sci. 14 (2) (2018) 156–164.
[19] S. Baba, G. Motomura, S. Ikemura, Y. Kubo, T. Utsunomiya, H. Hatanaka, et al., Quantitative evaluation of bone-resorptive lesion volume in osteonecrosis of the femoral head using micro-computed tomography, Joint Bone Spine. 87 (1) (2020) 75–80.
[20] J. Gardeniers, ARCO committee on terminology and staging. Report on the committee meeting at Santiago de Compostella, ARCO Newsl. 5 (5) (1993) 79–82.
[21] C. Mourad, K. Laperre, M. Halut, C. Galant, M. Van Cauter, B.C. Vande Berg, Fused micro-computed tomography (μCT) and histological images of bone specimens, Diagn Interv Imaging. 99 (7–8) (2018) 501–505.
[22] D. Resnick, G. Niwayama, R.D. Coutts, Subchondral cysts (geodes) in arthritic disorders: pathologic and radiographic appearance of the hip joint, AJR Am. J. Roentgenol. 128 (5) (1977) 799–806.
[23] M. Catto, The histological appearances of late segmental collapse of the femoral head after transcervical fracture, The Journal of bone and joint surgery British volume. 47-B (4) (1965) 777–791.
[24] S.Y. Wong, J. Kariks, R.A. Evans, C.R. Dunstan, E. Hills, The effect of age on bone composition and viability in the femoral head, J. Bone Joint Surg. Am. 67 (2) (1985) 274–283.
[25] D. Altman, Practical statistics for medical research., Chapman and Hall, London, Stat. Med. 10 (10) (1991) 1635–1636 1991.
[26] J.E. Kenzora, M.J. Glimcher, Pathogenesis of idiopathic osteonecrosis: the ubiquitous crescent sign, Orthop Clin North Am. 16 (4) (1985) 681–696.
[27] P.G. Bullough, E.F. DiCarlo, Subchondral avascular necrosis: a common cause of arthritis, Ann. Rheum. Dis. 49 (6) (1990) 412–420.
[28] K. Karasuyama, T. Yamamoto, G. Motomura, K. Sonoda, Y. Kubo, Y. Iwamoto, The role of sclerotic changes in the starting mechanisms of collapse: a histomorphometric and FEM study on the femoral head of osteonecrosis, Bone. 81 (2015) 644–648.
[29] K.B. Broberg, Introduction, in: K.B. Broberg (Ed.), Cracks and Fracture, Academic Press, San Diego, 1999, pp. 1–4.
[30] B.M. Maldague, Le diagnostic radiologique précoce de la nécrose aseptique post-traumatique de a tête fémorale, J Acta orthop belg. 50 (1984) 324–342.
[31] H.A. Sissons, M.A. Nuovo, G.C. Steiner, Pathology of osteonecrosis of the femoral head, Skelet. Radiol. 21 (4) (1992) 229–238.
[32] B.A. Lakin, H. Patel, C. Holland, J.D. Freedman, J.S. Shelofsky, B.D. Snyder, et al., Contrast-enhanced CT using a cationic contrast agent enables non-destructive assessment of the biochemical and biomechanical properties of mouse tibial plateau cartilage, J. Orthop. Res. 34 (7) (2016) 1130–1138.
[33] S. de Bournonville, S. Vangrunderbeeck, G. Kerckhofs, Contrast-enhanced MicroCT for virtual 3D anatomical pathology of biological tissues: a literature review, Contrast Media Mol Imaging. 2019 (2019) 8617406.